Aromaticity of Singlet and Triplet Boron Disk-like Clusters: A Test for Electron Counting Aromaticity Rules

Slađana Đorđević,[1] Miquel Solà,[2] Slavko Radenković[1]*

[1]*University of Kragujevac, Faculty of Science, P. O. Box 60, 34000 Kragujevac, Serbia*

[2]*Institute of Computational Chemistry and Catalysis and Department of Chemistry, University of Girona, C/ M. Aurèlia Capmany, 69, 17003 Girona, Catalonia, Spain*

Abstract

Boron clusters are polyhedral boron containing structures that have unique features and properties. The disk-like boron clusters are among the most fascinating boron cluster forms. These clusters have a molecular orbital distribution similar to the one derived from the simple particle-on-a-disk model. In this model, the molecular orbitals come by pairs except for m = 0. Disk-like boron clusters in their singlet ground state are aromatic when they reach a closed-shell structure. One could expect that disk-like aromatic boron clusters in the singlet state, when acquiring or releasing two electrons, may be also aromatic in the lowest-lying triplet state. We use magnetically induced current densities and bond current strengths to analyze the aromatic character of a series of disk-like boron clusters. Our results show that, with the exception of triplet $^3B_{19}^-$, the disk-like boron clusters follow Hückel and Baird's rules if one considers the different molecular orbitals grouped by its symmetry. We also found that, if the lowest-lying triplet state in disk-like boron clusters is aromatic, this triplet state is the ground state for this species.

INTRODUCTION

Bare boron clusters have gained a lot of attention in the past few decades from both experimental and theoretical chemists.[1–5] Elemental boron clusters were found to exist in a wide range of different geometrical forms, thanks to an electron deficient nature of boron and its affinity to create multicentred chemical bonds.[6–8] There is a continuous development of procedures for the synthesis of pure and functionalized boron clusters.[9,10] Due to appearance in such diverse spatial and electronic structures, boron clusters became interesting for applications in many fields, such as development of new bioactive,[11–17] magnetic,[18,19] semiconductive,[20] superconductive[21] and hydrogen storage materials.[22–24]

Understanding of the electronic structure and chemical bonding in boron clusters has emerged as a very challenging task.[25–29] The aromaticity has been widely employed to rationalize the structure, reactivity and stability of boron clusters.[30–34] The studies of electronic properties of boron-based complexes brought further evolvement of the aromaticity concept. Boron clusters can exhibit aromaticity, antiaromaticity, disk, double or even conflicting aromaticity.[2,30,35] The aromaticity concept is traditionally related to organic molecules, and several simple electron counting rules have been established, which can instantly provide molecular aromaticity characterization.[36,37] The well-known Hückel's rule states that the $4n+2$ monocyclic annulenes exhibit aromaticity while $4n$ ones exhibit antiaromaticity.[38] The Baird's rule predicts the reversed aromatic properties of the lowest-lying triplet state of annulenes.[39,40] The Hückel and Baird's rules have been successfully extended and applied to many other organic and inorganic systems, including boron-based clusters.[36,41] For some of boron clusters it has been shown that the Hückel's rule can give wrong characterization of molecular aromaticity.[26,42,43] It is worth mentioning that it has been shown that the Hückel and Baird's rules can be viewed as being a part of a more general rule which considers separate contributions of α and β electrons.[44] As Mandado and his coworkers[44] have proposed, systems with an odd number of α (or β) π electrons are α (or β) aromatic, while those with an even number of α (or β) π electrons are α (or β) antiaromatic. This counting rule has been successfully applied to rationalize the magnetic properties of aromatic species.[45] We are grateful for an anonymous referee for calling our attention to the recent work of Valiev *et al.*[46] in which the Hückel and Baird's rules have been unified and reformulated in terms of the number of doubly and singly occupied orbitals: molecules are aromatic (respectively

antiaromatic) if they have an odd (respectively even) number of doubly and singly occupied conjugated valence orbitals.

It has been shown that disk-like boron clusters exhibit a singlet ground state, and their aromaticity was described by introducing the so-called disk aromaticity concept.[28,47–49] Furthermore, the studied systems are characterized by a unique dynamical behavior. In particular, B_{13}^+, B_{19}^-, and B_{20}^{2-} show an almost free rotation of the inner unit relative to the outer ring.[47,50–52] Previously it has been demonstrated that some of boron-based complexes can have a triplet ground state.[1,2] Because the rules of aromaticity followed by classical organic aromatic monocycles in their ground and lowest-lying triplet states, i.e, the Hückel and Baird rules, differ from those followed by disk-like boron clusters, we wonder whether disk-like boron clusters that are aromatic in their ground states remain aromatic in their lowest-lying triplet states when the number of valence electrons is increased or reduced by two electrons. So, we would like to answer the question whether a similar rule as the Baird rule is applicable to disk-like boron clusters. We expect this could be the case because the molecular orbitals in the particle-on-a-disk model come by pairs except for m = 0.[48] The disk-like boron clusters discussed here are depicted in Fig. 1. The complete set of the studied complexes is given in Fig. S1 and in Table 1. We consider the ground state of these boron cluster and the lowest-lying triplet state of their dications and dianions.

The characterization and rationalization of aromaticity in disk-like boron clusters is challenging due to simultaneous out-of-plane (π) and in-plane (σ) bonding in these complexes. While properties of the π-electron subsystem in the studied complexes are well understood, the description of the σ electron subsystem was found to be very challenging. For instance, B_{19}^- has 58 valence electrons, of which 12 belong to π-system and the remaining 46 to σ-system. Using the adaptive natural density partitioning (AdNDP) method,[53] Yan *et al.*[27] have showed that 26 σ electrons contribute to the bonding along the outer B_{13} ring, 10 σ electrons are delocalized inside the pentagonal B_6 unit and the rest 10 σ electrons are delocalized between the inner and outer rings. Recently, using the AdNDP and canonical molecular orbital (CMO) analysis, Li *et al.*[29] have proposed somewhat different bonding situation in B_{19}^- claiming that there are 6 σ electrons delocalized inside the central B_6 unit and 14 σ electrons which are delocalized between the inner and outer rings.

In this work we provide a rationalization of the electronic structure of the studied disk-like boron clusters based solely on the CMOs and their nodal characteristic, as originally proposed in

the disk aromaticity model.[47,48] To the best of the authors' knowledge, for the first time the aromatic character for each of σ and π electron subshells in the studied boron disks was thoroughly studied based on the magnetically induced current densities.[54–56] As will be shown below the studied series of complexes (Fig. S1) consists of both singlet and triplet ground state systems, which provides a relevant set to test applicability of electron counting aromaticity rules.

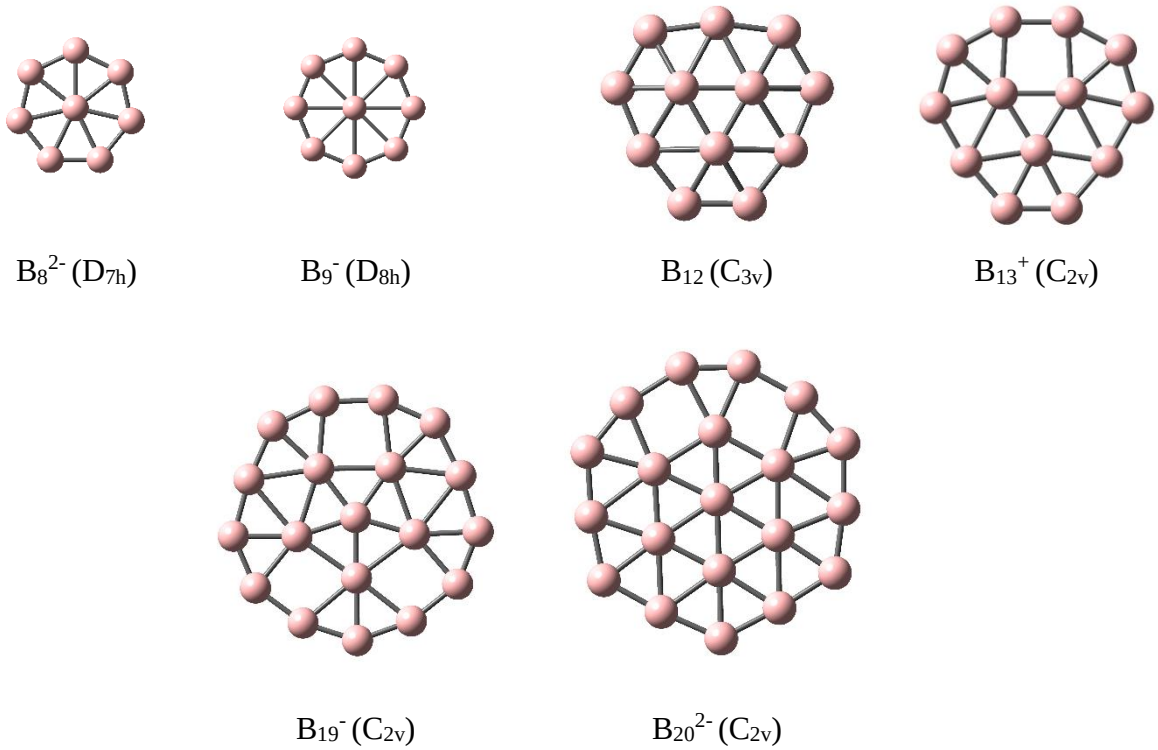

Figure 1. Set of the studied boron disk-like clusters.

COMPUTATIONAL DETAILS

Geometries of the complexes depicted in Fig. 1 were fully optimized at the B3LYP/def2-TZVP level in singlet spin states by employing the Gaussian 09 program.[57] Starting from the so-obtained geometries the cluster charge was increased/decreased by 2 and subsequently the geometry optimizations were carried out in both singlet and triplet spin states. Only systems whose absolute charge does not exceed 2 were considered, because systems with higher charges have no practical chemical relevance. For instance, based on B_{20}^{2-} cluster in Fig. 1, we considered B_{20} but not B_{20}^{4-}. Frequency calculations confirmed that the obtained optimized structures have no imaginary frequencies.

The geometry optimizations and current density calculations were carried out using the spin unrestricted and spin restricted formalisms for triplet and singlet states of the examined clusters, respectively. Magnetically induced current densities were calculated at the B3LYP/def2-TZVP level of theory using the diamagnetic zero variant of the continuous transformation of origin of current density method (CTOCD-DZ).[58–61] The external magnetic field was set to be perpendicular to the molecular plane of the studied complexes. In the case of non-planar systems, the external magnetic field was applied perpendicular to the plane which maximize the projection area of the given molecule. The current densities were calculated and mapped 1 bohr above the surface which approximately adopts the shape of the boron clusters. Consequently, all possible visual confusions coming from the strong localized σ electron currents induced in the molecular plane were eliminated. In this work the current density maps were used as a qualitative tool, whereas detailed quantitative information on the induced current densities were obtained by calculations of the integrated bond current strengths. The calculated current densities were visualized using the Paraview program.[62] In the current density maps, diatropic (respectively paratropic) current densities were represented by counterclockwise (respectively clockwise) circulations. Bond current strengths were calculated using the disk-based quadrature scheme.[63] This method is based on numerical integration[64] of the current densities that pass through a disk, which perpendicularly bisects the middle of the considered bond. In the case of σ electron bond current strengths, the integration disk was centered along the bond direction and the radius of the integration disk was the boron atom covalent radius.[65] For π electron bond current strengths, the integration surface was divided into two disks, one above and one below the molecular plane. The total integration surfaces for σ and π electron bond current strength calculations were set to be equal. This was our choice, although we are aware that using different integration surfaces one can get different bond current strengths. All current density calculations were carried out by our in-house FORTRAN program.

RESULTS

The optimized structures of the studied disk-like boron complexes are depicted in Fig. S1. All systems shown in Fig. 1 were found to be planar, except B_{12} which adopts a bowl-shaped C_{3v} structure, which is in agreement with previous studies.[1,28,49] The systems obtained from the complexes given in Fig. 1 by changing their charge were found to be more stable in triplet than in

singlet spin state. In particular, the optimized geometries of singlet and triplet B_8, B_9^+, B_{12}^{2-}, B_{12}^{2+}, B_{13}^-, B_{19}^+, and B_{20} and the respective adiabatic singlet-triplet energy gaps obtained at the B3LYP/def2-TZVP level of theory are provided in Fig. S2. Among the triplet clusters shown in Fig. S1 only $^3B_{12}^{2+}$ has a non-planar structure. The singlet-triplet energy gap for the examined clusters ranges from 8.6 to 50.2 kJ/mol. In the case of B_{19}^+ and B_{20}, the obtained triplet state geometries do not correspond to the global minimum structures which were previously characterized and found to not have disk-like shapes (we have only considered disk-like boron clusters).[66,67] It has been shown that boron clusters up to 18 atoms favor planar structures, whereas those with more than 18 atoms generally prefer 3D structures.[68]

All studied disk-like complexes (Fig. S1) are characterized by 3n - q valence electrons, where n and q represent the number of boron atoms and the cluster charge, respectively. It should be noted that the σ-π notation sometimes can be misleading, but here the σ and π MOs are those which are, respectively, symmetric and antisymmetric with regard to reflection in the molecular plane. This kind of notation was employed in all previous studies of the disk-like boron clusters.[26,47,48] Although some of the examined clusters were found to deviate from planarity, in all cases using a simple visual inspection it was possible to clearly distinguish between σ- and π-type CMOs. Thereafter, the total numbers of σ and π electrons were easily determined (Table 1). It has been shown that there is a one-to-one correspondence between MOs of the boron disk clusters and the eigenfunctions of a particle-in-a-circular-box.[26,48] The eigenstates of the particle-on-a-disk model are determined by the combination of the radial (n = 1, 2, 3,…) and angular (m = 0, ±1, ±2, ±3,…) quantum numbers. For each of σ and π MOs the quantum numbers n and m were determined based on their nodal characteristics, i. e. by counting the numbers of the respective radial and angular nodes. In particular, the particle-on-a-disk model predicts that each MO is characterized by n – 1 radial nodes and |m| angular nodes. The σ and π CMOs having the same number of radial nodes were grouped into σ_n and π_n subsystems. Within each of σ_n and π_n subgroups non-(quasi)-degenerated CMOs differ by the number of angular nodes (|m|).

Table 1. Partitioning the total number of valence electrons into σ and π contributions, which are further dissected into σ_n and π_n subgroups based on the respective number of radial nodes (n - 1).

	N_{total}	$N_{\sigma\ total}$	N_{σ_1}	N_{σ_2}	N_{σ_3}	$N_{\pi\ total}$	N_{π_1}	N_{π_2}
B_8^{2-}	26	20	14	6		6	6	
$^3B_8$	24	20	14	6		4	4	
B_9^-	28	22	16	6		6	6	
$^3B_9^+$	26	22	16	6		4	4	
B_{12}	36	30	18	10	2	6	6	
$^3B_{12}^{2-}$	38	30	18	10	2	8	8	
$^3B_{12}^{2+}$	34	28	18	8	2	6	6	
B_{13}^+	38	32	20	10	2	6	6	
$^3B_{13}^-$	40	32	20	10	2	8	8	
B_{19}^-	58	46	26	14	6	12	10	2
$^3B_{19}^+$	56	46	26	14	6	10	9	1
B_{20}^{2-}	62	50	26	14	10	12	10	2
$^3B_{20}$	60	48	26	14	8	12	10	2

As an illustrative example, Fig. 2 shows valence CMOs for B_{13}^+. There are 6 π electrons populating 3 CMOs, all of which have 0 radial nodes (n = 1), and therefore these orbitals belong to the π_1 subgroup (Fig. 2). Completely analogous analysis can be extended to σ electron subsystem. However, it should be noted that in general σ-type CMOs may appear as more complex since they come from the 2s-$2p_x$-$2p_y$ mixing, whereas π CMOs are solely based on $2p_z$-atomic orbitals. In any case, the nodal characteristics of σ-type CMOs can be recognized. It was found that in B_{13}^+ there are 10 σ orbitals with zero radial nodes (σ_1), 5 σ orbitals with 1 radial node (σ_2) and 1 σ CMO with 2 radial nodes (σ_3). The electron population of all σ and π subgroups in B_{13}^+ is listed in Table 1. The corresponding analysis was performed for all studied boron clusters and the obtained results are summarized in Table 1 and Figs. S3-S14. As a general rule, it was found that for all examined systems the number of σ_1 electrons is twice the number of B-B bonds along the peripheral ring. This finding can be rationalized using the AdNDP bond analysis which showed that for all disk-like clusters having n_{out} B atoms along the most outer ring there are exactly $2n_{out}$ σ 2c-2e B-B bonds.[27,29] The population of other subshells can also be predicted by the simple counting rules which has been previously formulated.[26]

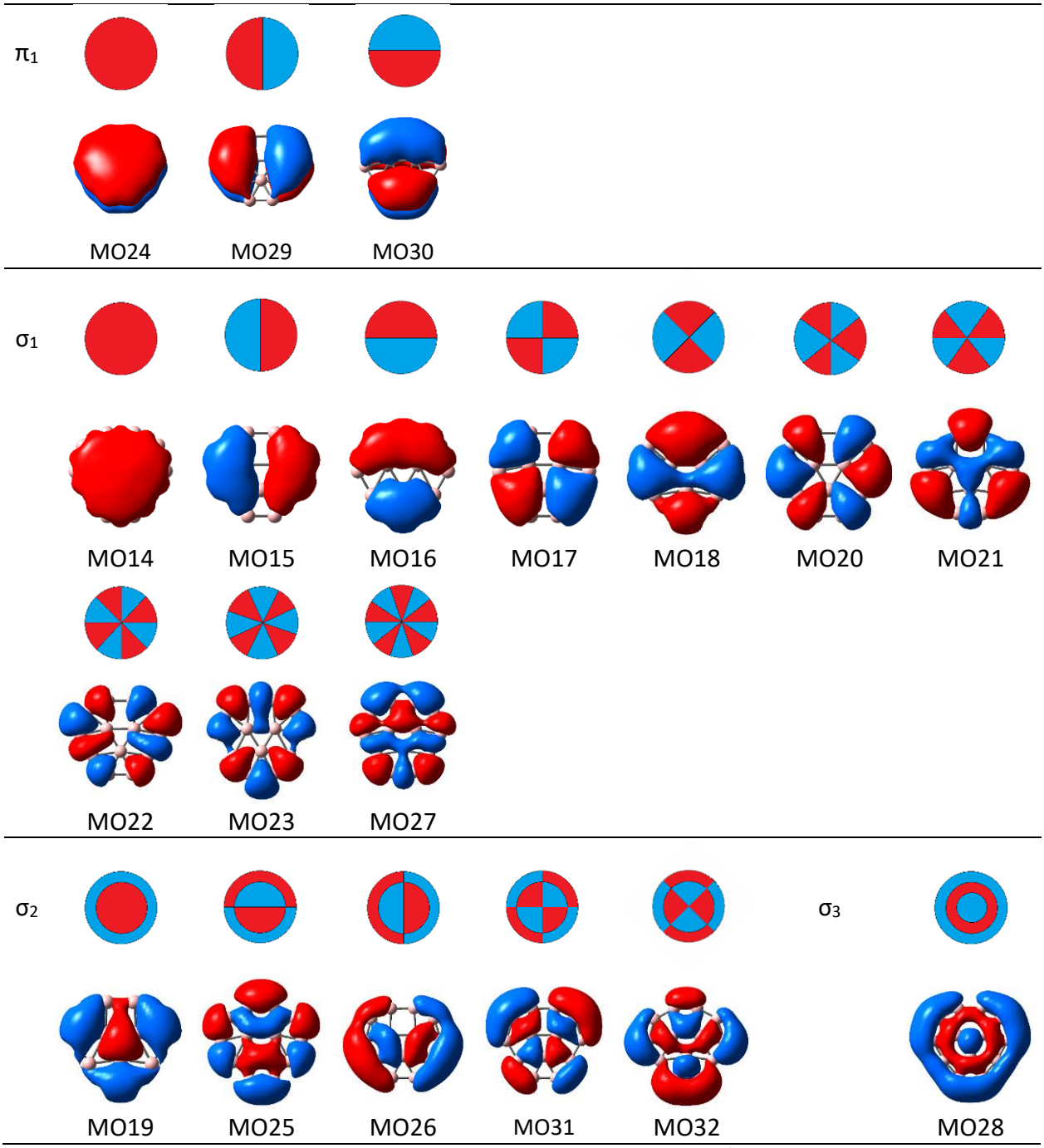

Figure 2. Valence canonical molecular orbitals (CMOs) of B_{13}^{+} partitioned into σ_n and π_n subgroups based on the respective number of radial nodes (n - 1).

In the following discussion the studied boron clusters were grouped based on similarities in their electronic and geometrical characteristics. For all systems the current density contributions coming from each of σ_n and π_n subsystems were analyzed. The CTOCD-DZ method provides a

connection between the induced current density and electronic structure of a given molecule in the following way: diatropic (respectively paratropic) current density comes from the virtual translational (respectively rotational) orbital transitions. The contribution of the given orbital transition is also determined by the corresponding energy gap. As the energy difference between the occupied and unoccupied orbitals increases the contribution of the transition becomes smaller. Therefore, the origin of the current density can be explained based on only a few electrons in orbitals close to the HOMO level. If these symmetry- and energy-based selection rules are applied for the centered systems, such are the studied boron clusters, one can reformulate them in terms of the number of the orbital angular nodes: excitations for which an occupied orbital having one angular node less than the corresponding virtual orbital give diatropic currents, whereas those excitations preserving the number of angular nodes give paratropic currents. For instance, using these rules one can expect that in all examined systems the σ_1 subshell will give very weak currents since this subshell is completely filled, and there are no possible excitations within the subshell. Our calculations confirmed that the σ_1 subsystem gives negligible current density contributions, and for this reason the aromatic character of this part of σ-type CMOs was excluded from the following analysis. The selection rules can be used to qualitatively predict the current density contributions of other σ_n and π_n subshells (Fig. S15). Based on the particle-on-a-disk model for each of these electronic subsystems molecular orbitals come in pairs, except for m = 0. Therefore, in the σ_n and π_n subshells having a closed-shell configuration with 2k + 2 electrons (2, 6, 10, 14, …) only the translational excitation HOMO to LUMO (increasing the number of angular nodes by one) is possible, and these subshells will give diatropic currents. The same selection rules can be applied for open-shell subshells. Within the unrestricted electronic-structure formalism alpha and beta electrons occupy two separate stacks, and only allowed excitations are those within the given stack. Thereafter, within α (or β) σ_n and π_n subshells with 2k + 1 electrons (1, 3, 5, 7, …) only translational excitations (increasing the number of angular nodes by one) are possible, and these subshells will give diatropic current contributions. On the other hand, if the number of α (or β) electrons in a subshell is even (2, 4, 6,…) the dominant transition is between orbitals having the equal number of angular nodes (same |m|), and such α (or β) subshell will give paratropic currents. This way, the applicability of the Hückel, Baird, and Mandado's rules for the studied boron disk-like clusters can be rationalized based on combining symmetry, energy, and spin selection rules which are applied to the particle-on-a-disk model (Fig. S15). In what follows we will test the

performance and limits of the particle-on-a-disk model in description of the electronic structure of the disk-like boron clusters.

B_8^{2-}, $^3B_8$, B_9^-, $^3B_9^+$.

B_8^{2-} and B_9^- clusters exhibit very similar geometric and electronic properties. Both systems have planar molecular wheel structure in which the central boron atom is hepta- and octa-coordinated. If the σ_n and π_n subsystems are compared for B_8^{2-} and B_9^-, the only difference is found in the population of σ_1 subsystem, which can be explained by different size of the outer rings in these systems.

Figs. 3 and 4 show the maps of the induced current densities separated into contributions of π_1 and σ_2 subsystems. The bond current strengths were separately calculated for σ_2 and π_1 subsystems as the average of all B-B bonds involved in the outer ring (Table 2). For the sake of comparison, the π electron bond current strength for benzene was calculated at the same level of theory (6.7 nA T^{-1}). The intensity and distribution of the induced current densities are very similar in B_8^{2-} and B_9^-, as well as in $^3B_8$ and $^3B_9^+$. It was found that π_1 and σ_2 subsystems in B_8^{2-} and B_9^- induce strong diatropic currents. The nature of the obtained current densities can be rationalized with Hückel's rule, as each of π_1 and σ_2 in B_8^{2-} and B_9^- have 6 electrons. It should be noted that this has been previously shown by Fowler *et al*.[69]

In the triplet $^3B_8$ and $^3B_9^+$ the σ_2 subsystem keeps the closed-shell configuration with 6 electrons as in the parent B_8^{2-} and B_9^- clusters. It was found that the σ_2 subsystem induces diatropic current densities in agreement with Hückel's rule. As can be seen from Table 2, the intensity of the σ_2 subsystem currents is very similar in all clusters shown in Figs. 3 and 4. On the other hand, the π_1 subgroup has an open-shell configuration with 4 electrons in both the lowest-lying triplet states of $^3B_8$ and $^3B_9^+$, and this electronic subsystem induces diatropic currents which can be explained by Baird's rule. Figs. 3 and 4 and the data from Table 2 show that the intensities of the π_1 subsystem currents in $^3B_8$ and $^3B_9^+$ are weaker than that in B_8^{2-} and B_9^-.

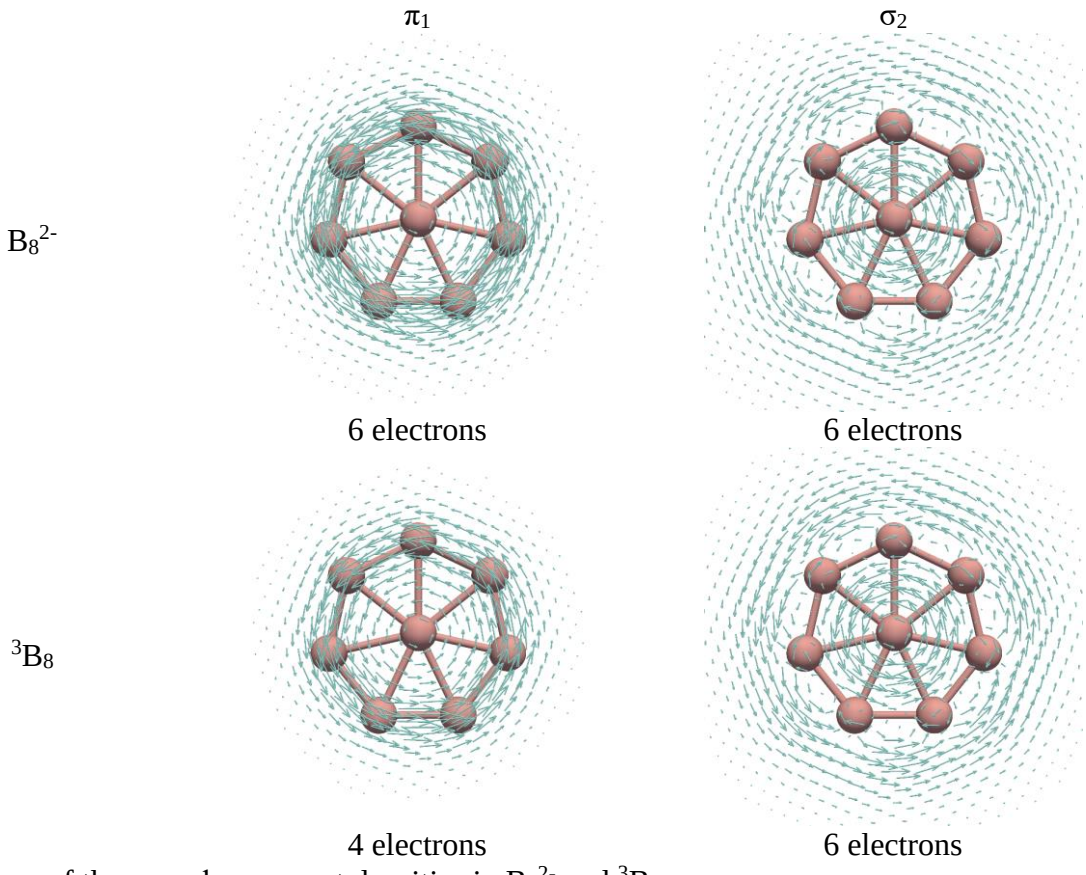

Fig. 3 Maps of the π_1 and σ_2 current densities in B_8^{2-} and $^3B_8$.

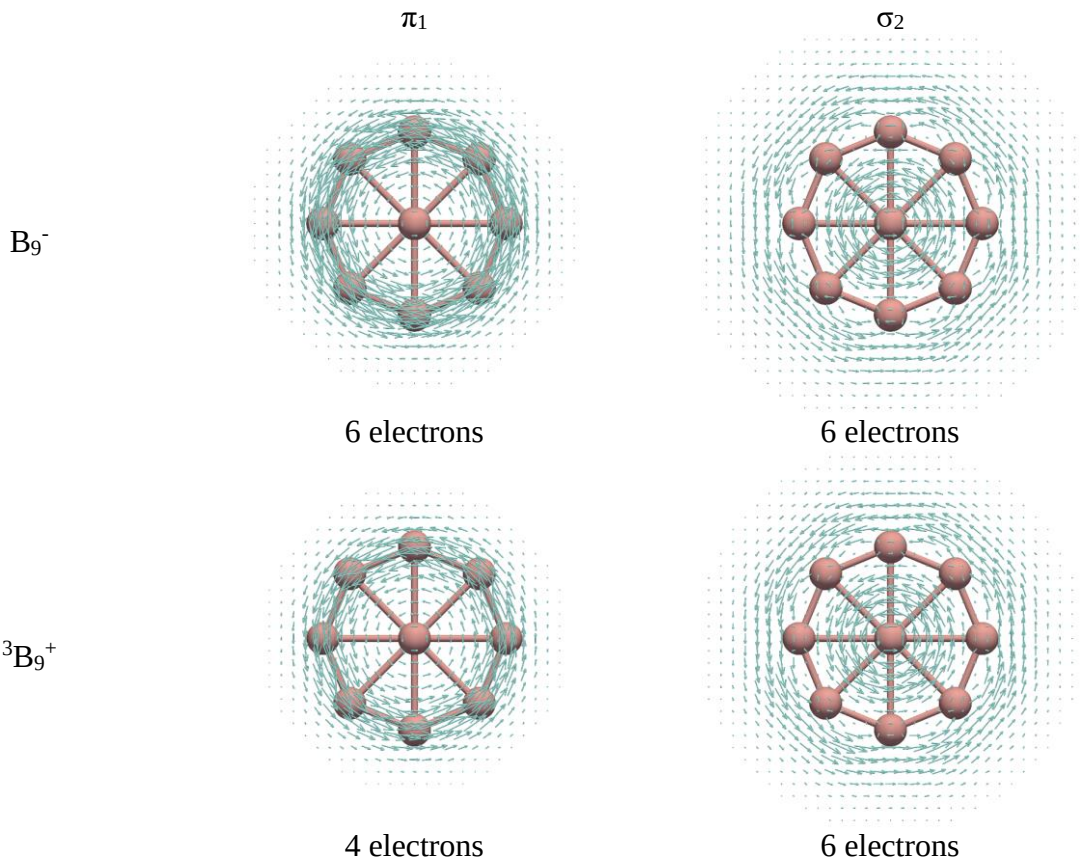

Fig. 4 Maps of the π_1 and σ_2 current densities in B_9^- and $^3B_9^+$.

Table 2. Bond current strengths (nA T^{-1}) calculated as the average of all B-B bonds involved in the given inner/outer ring of the studied clusters.

	ring	σ_2	σ_3	π_1	π_2
B_8^{2-}		4.8		6.0	
$^3B_8$		5.1		4.1	
B_9^-		4.6		6.3	
$^3B_9^+$		4.6		4.2	
B_{12}	inner	1.9	0.3	1.1	
	outer	3.8	0.2	3.6	
$^3B_{12}^{2-}$	inner	2.7	0.2	1.2	
	outer	4.5	0.01	6.2	
$^3B_{12}^{2+}$	inner	1.4	0.4	0.3	
	outer	1.6	0.4	2.8	
B_{13}^+	inner	3.0	0.4	1.2	
	outer	4.8	0.4	4.2	
$^3B_{13}^-$	inner	3.0	0.3	1.0	
	outer	5.2	0.3	5.1	
B_{19}^-	inner	5.9	1.4	1.9	1.3
	outer	5.2	1.0	6.0	0.6
$^3B_{19}^+$	inner	6.5	1.2	-3.6	0.5
	outer	4.7	1.1	-6.5	0.3
B_{20}^{2-}	inner	2.0	-7.6	3.3	0.9
	outer	2.5	0.6	7.3	0.7
$^3B_{20}$	inner	2.4	-1.9	3.9	0.6
	outer	2.0	1.6	6.7	0.7

B_{12}, $^3B_{12}^{2-}$, $^3B_{12}^{2+}$, B_{13}^+, $^3B_{13}^-$.

B_{12} and B_{13}^+ feature the central three-membered ring surrounded by the nine- and ten-membered outer rings, respectively. While B_{13}^+ is planar, B_{12} has a bowl-like shape (Fig. S1).[1,28,49] The different size of the outer ring causes different population of the σ_1 subshell (18 and 20 electrons in B_{12} and B_{13}^+, respectively). The π_1, σ_2, and σ_3 subsystems have 6, 10 and 2 electrons in B_{12} and B_{13}^+, respectively (Table 1). As can be seen from Figs. 5 and 6 the π_1 and σ_2 subsystems induces diatropic circulations, whereas the σ_3 subsystem shows very weak currents in B_{12} and B_{13}^+. The obtained current density maps are in line with the Hückel rule predictions. The bond current strengths were calculated as the average of all B-B bonds in the outer and inner rings (Table 2). These data also demonstrate that the extent of the induced currents in B_{12} and B_{13}^+ are very similar for all dissected CMOs subgroups.

In the triplet $^3B_{12}^{2-}$ and $^3B_{13}^-$ the σ_2 and σ_3 subsystems have the same populations as in B_{12} and B_{13}^+, while the additional 2 electrons are in the π_1 subshell which has an open-shell configuration with 8 electrons. Figs. 5 and 6 demonstrate that the π_1 electrons show magnetically aromatic behavior as predicted by Baird's rule. The currents induced by the π_1 subsystem in $^3B_{12}^{2-}$ and $^3B_{13}^-$ are stronger than that in B_{12} and B_{13}^+.

In the triplet $^3B_{12}^{2+}$ the unpaired electrons reside in the σ_2 subsystem, which has 8 electrons and sustain diatropic currents in agreement with Baird's rule. On the other hand, π_1 and σ_3 subsystems exhibit the closed-shell configuration with the same number of electrons (Table 1), and very similar magnetic response as in B_{12} (Table 2).

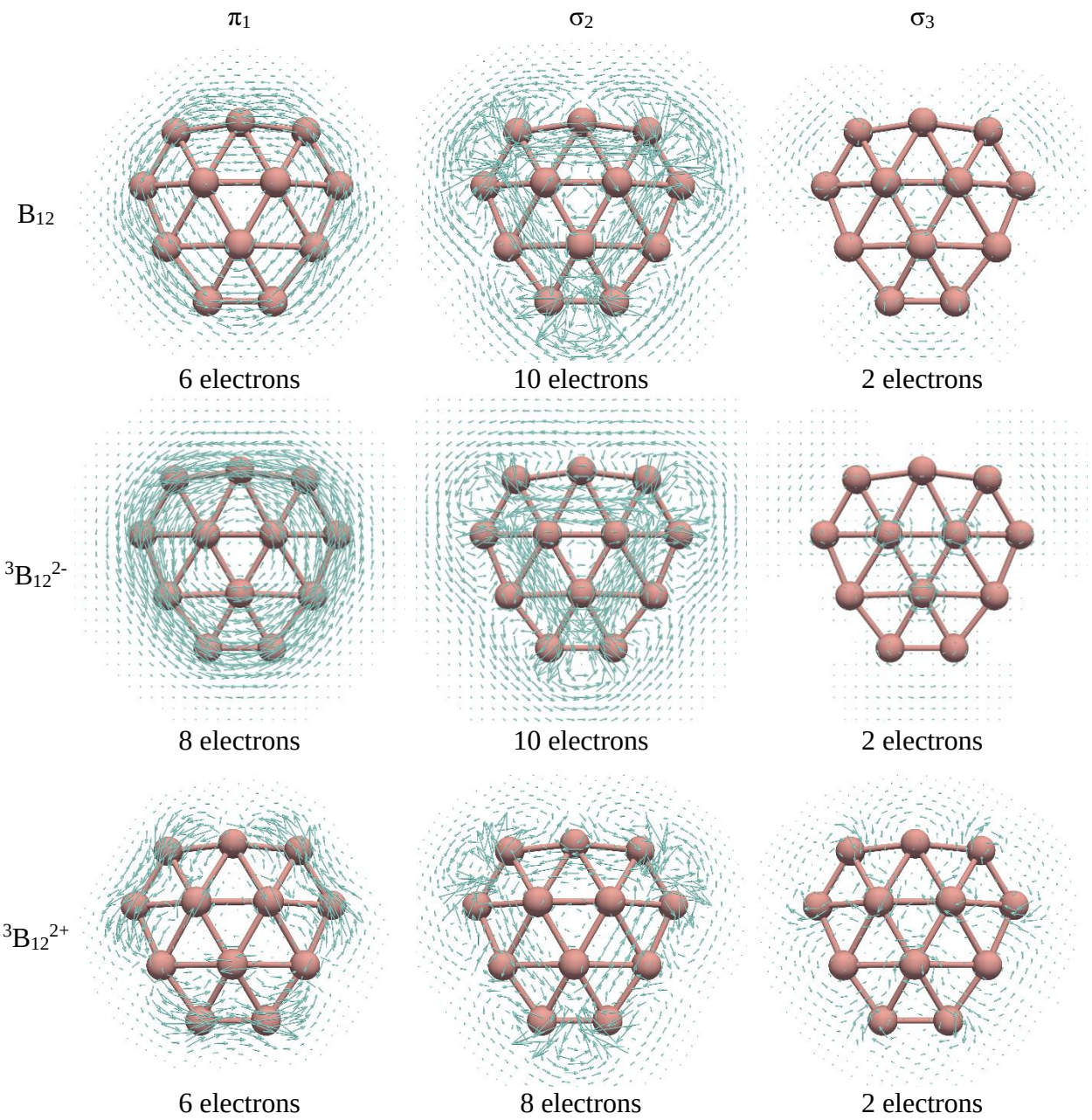

Fig. 5 Maps of the π_1, σ_2, and σ_3 current densities in B_{12}, $^3B_{12}^{2-}$, and $^3B_{12}^{2+}$.

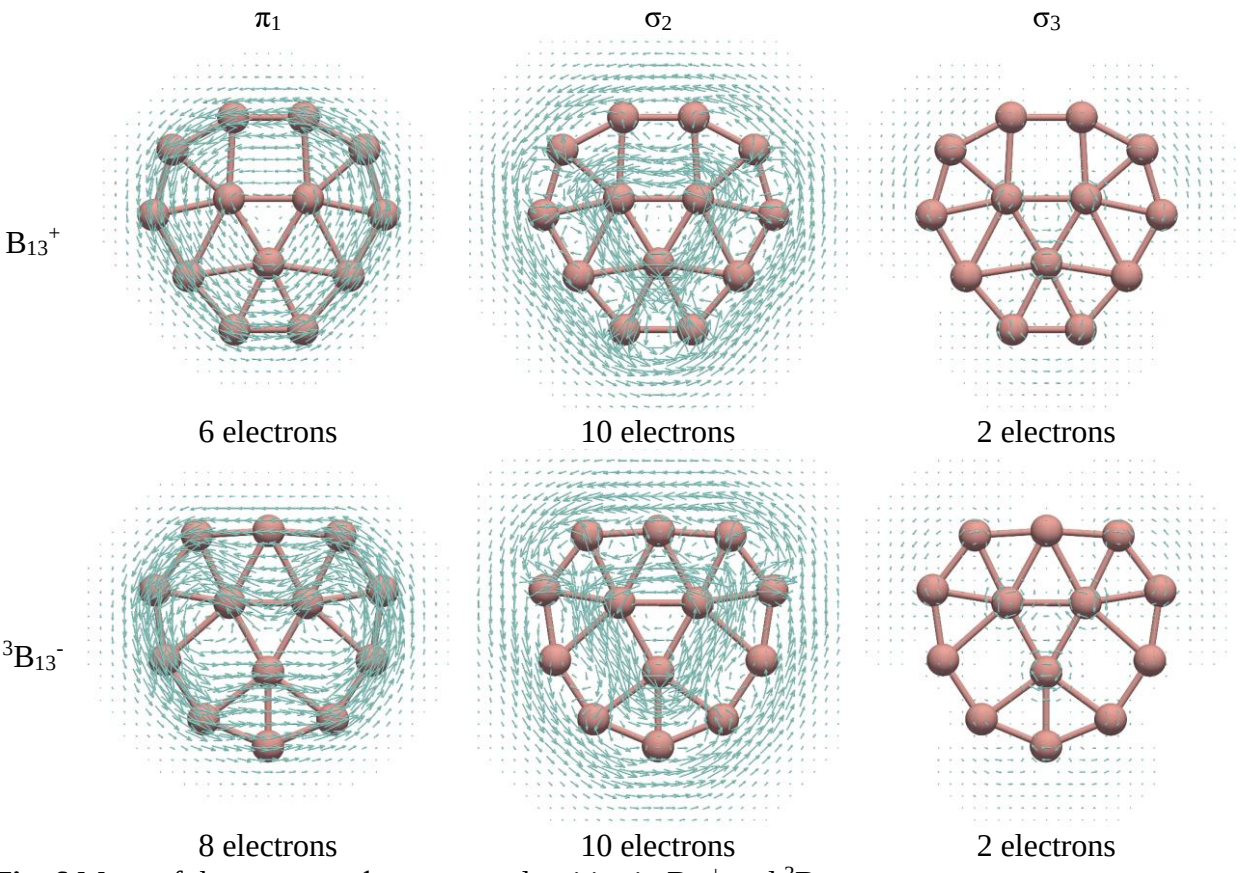

Fig. 6 Maps of the π_1, σ_2, and σ_3 current densities in B_{13}^+ and $^3B_{13}^-$.

B_{19}^- , $^3B_{19}^+$.

B_{19}^- has the planar structure in which the pentagonal B_6 unit is enclosed by the other thirteen boron atoms. In B_{19}^- π CMOs can be divided into two groups based on the number of radial nodes: π_1 with 10 electrons and π_2 with 2 electrons (Table 1 and Fig. S11). The σ system is described through σ_1, σ_2, and σ_3, having 26, 14, and 6 electrons, respectively. The bond current strengths were calculated for the outer 13-membered and inner 5-membered rings separately as the average value of all bonds in the given ring (Table 2). The current density analysis shown in Fig. 7 and in Table 2 revealed that all π and σ subsystems induce diatropic circulations, which is in agreement with the Hückel rule. The most intense current density comes from π_1 and σ_2 subsystems, whereas π_2 and σ_3 exhibit much weaker currents. In the triplet $^3B_{19}^+$, all σ subshells have the closed-shell configuration with the same population as in B_{19}^-. The main difference between $^3B_{19}^+$ and B_{19}^- is found for the π electron system. In particular, there are 9 electrons occupying π_1, and 1 electron in π_2 subsystem of $^3B_{19}^+$. If one compares current densities in B_{19}^- and $^3B_{19}^+$, it can be seen that σ electrons induce very similar currents in both systems. On the other hand, the π_1 subsystem in $^3B_{19}^+$ sustains strong paratropic current densities. The triplet $^3B_{19}^+$ cluster reveals a limitation of the Hückel and Baird's rules, which can be applied only for systems with even number of electrons. On the other hand, Mandado's rule correctly predicts that 5 α electrons will give diatropic, while 4 β electrons of the π_1 subsystem will give paratropic currents (Fig. 8). The Mandado's rule can successfully be applied to the π_2 subsystem in $^3B_{19}^+$ having 1 α electron (Fig. 7). In any case, it can be seen that Mandado's rule correctly predicts α and β conflicting aromaticity of the π_1 subsystem in $^3B_{19}^+$, but this rule does not answer which of the spin component will dominate.

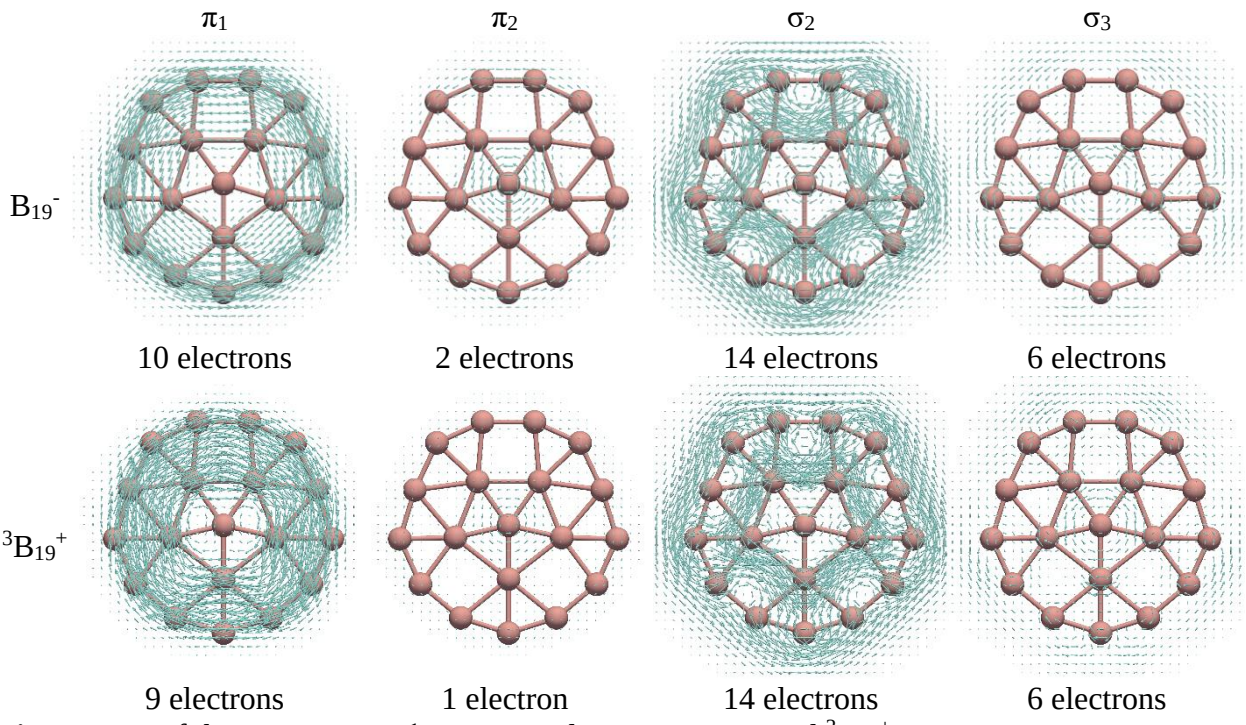

Fig. 7 Maps of the π_1, π_2, σ_2, and σ_3 current densities in B_{19}^- and $^3B_{19}^+$.

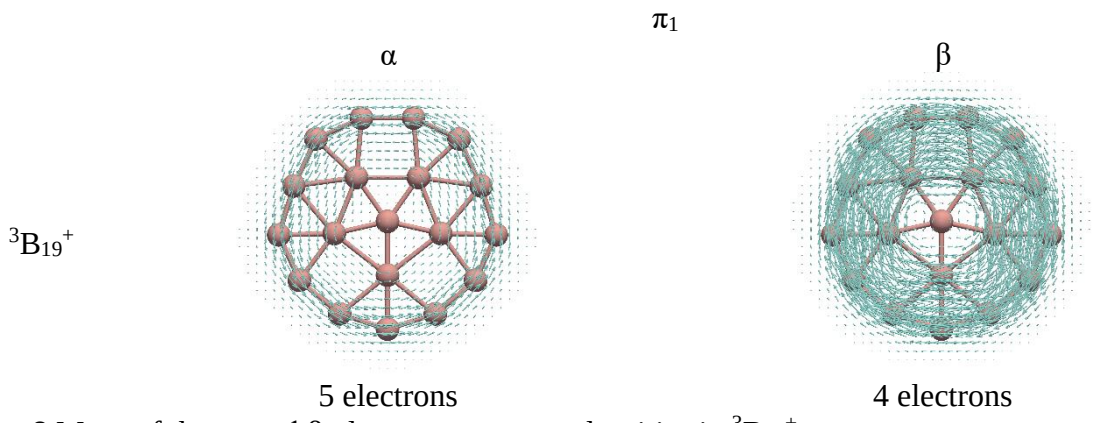

Fig. 8 Maps of the α- and β-electron π_1 current densities in $^3B_{19}^+$.

B_{20}^{2-}, $^3B_{20}$.

B_{20}^{2-} has a concentric ring structure, with the outer B_{13} ring and the inner hexagonal B_7 unit. The electronic features of B_{20}^{2-} appears to be very similar to those of B_{19}^-. The B_{20}^{2-} cluster, like B_{19}^-, has 10 and 2 electrons in π_1 and π_2, and 26 and 14 electrons in σ_1 and σ_2 subsystems. The main difference between B_{20}^{2-} and B_{19}^- comes from the σ_3 subshell which in the case of B_{20}^{2-} has 10 electrons. The same population of π subshells in B_{20}^{2-} and B_{19}^- leads to very similar intensities and distribution of the induced current densities (Figs. 7 and 9). On the other hand, the σ_2 and σ_3 subsystems in B_{20}^{2-} exhibit quite complex current density patterns. In both σ subsystems there are paratropic circulations around the central ring and diatropic circulations around the perimeter. The obtained current densities are in agreement with previous results for this complex,[48] and such magnetic behavior of σ subsystems cannot be rationalized by any of the existing counting rules of aromaticity. As can be seen from the current density maps (Fig. 9) and bond current strengths (Table 2), the σ_3 current density around the B_{13} ring in B_{20}^{2-} have strong local contributions around some of B-atoms, whereas the global circulation is rather weak. Our calculations showed that the most intensive contributions to the σ_3 subshell current density come from MO50 (HOMO – 1) and MO51 (HOMO). These two orbitals were formally assigned to the σ_3 subgroup, but it has been argued that these orbitals do not completely agree with the eigenfunctions predicted by the particle-on-a-disk model for n = 3 and m = ±2.[48] Actually, in B_{20}^{2-} (C_{2v}) there is a mixing of two states of the particle-on-a-disk model, one with n = 3, m = ±2 and the other with n = 2, m = ±4, from which MO50 (b_2) and MO51 (a_1), as well as their counterparts MO56 (b_2) and MO57 (a_1) are formed. In C_{2v} point group the in-plane translations have a_1 and b_2 symmetries, while the in-plane rotation has b_2 symmetry. The excitations MO50 → MO56 and MO51 → MO57 are translationally allowed (inducing diatropic currents) since the symmetry products $b_2 \times b_2$ and $a_1 \times a_1$ contain the symmetry of the in-plane translation (a_1). The excitations MO50 → MO57 and MO51 → MO56 are translationally (inducing diatropic currents) and rotationally allowed (inducing paratropic currents) because the symmetry product $b_2 \times a_1$ contains the symmetries of the in-plane translations and in-plane rotation (b_2). The $^3B_{20}$ cluster has the same population of the π_1, π_2, σ_1, and σ_2 subshells as in B_{20}^{2-}. The σ_3 subsystem in $^3B_{20}$ has the open-shell configuration with 8 electrons. This system gives much stronger diatropic currents around the B_{13} ring, and very weak paratropic currents in the central unit.

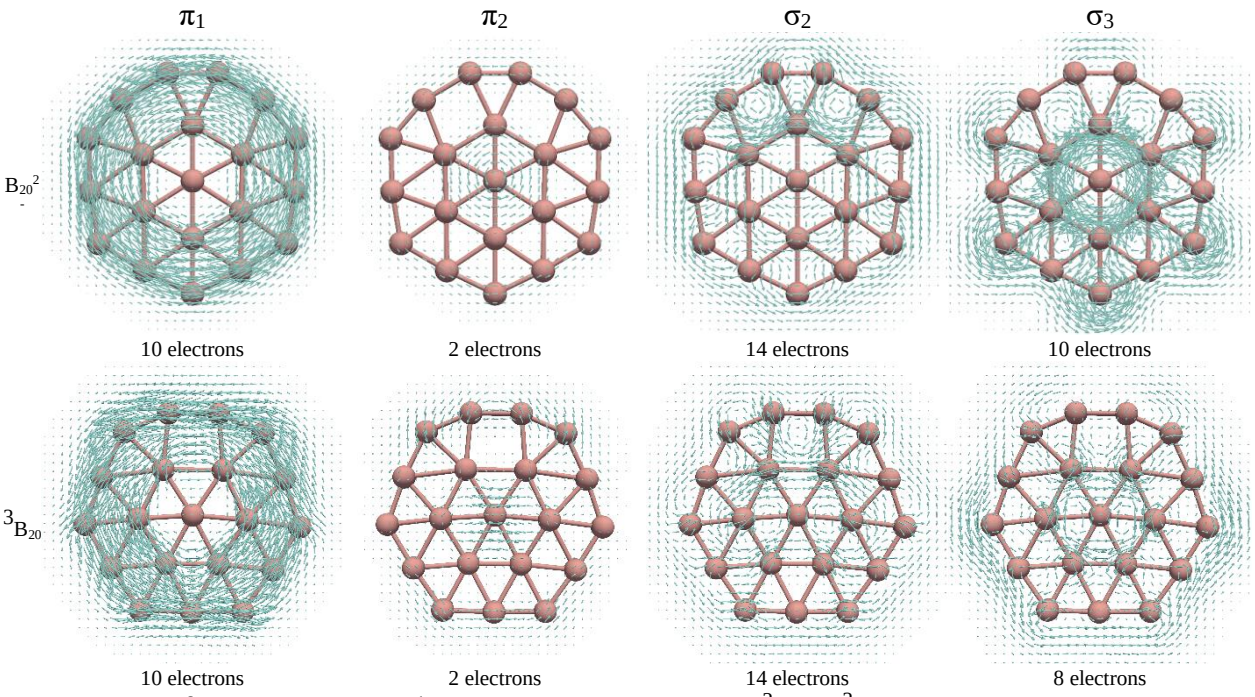

Fig. 9 Maps of the π_1, π_2, σ_2, and σ_3 current densities in B_{20}^{2-} and $^3B_{20}$.

CONCLUSIONS

In this work the electronic structure of a series of singlet and triplet disk-like boron clusters was examined by means of the CMO-based analysis, as proposed in the disk aromaticity model. The σ and π CMOs of the examined systems were grouped based on the number of their radial nodes. The calculated current densities demonstrated that the aromatic characteristics of σ and π electron subsystems in the singlet boron disks (Fig. 1) can be correctly predicted by the Hückel rule. The only exception was found for the singlet B_{20}^{2-} in which we found σ subshells that simultaneously induce diatropic and paratropic currents.

In the case of the triplet boron clusters with 8, 9, 12, and 13 boron atoms, the magnetic aromatic properties of the dissected σ and π electron subsystems was successfully rationalized by means of Hückel and Baird's rules. In the triplet $^3B_{19}^+$ cluster π electron system has an odd number of electrons, which requires employment of Mandado's rule.

The σ subsystems of B_{20}^{2-} and $^3B_{20}$ exhibit diatropic currents around the B_{13} ring, and paratropic currents in the central unit. Such a dual magnetic response cannot be rationalized by any of the existing electron counting rules of aromaticity.

ASSOCIATED CONTENT

Supporting Information. This information is available free of charge via the Internet at http://pubs.acs.org.

AUTHOR INFORMATION

Corresponding Author

*E-mail address: **slavkoradenkovic@kg.ac.rs**.

Notes

The authors declare no competing financial interest.

ACKNOWLEDGMENTS

S. Dj. and S. R. thank the Serbian Ministry of Education, Science and Technological Development (Agreement No. 451-03-68/2022-14/200122) for partial support of this work. M. S. is grateful for the financial support from the Ministerio de Ciencia e Innovación (PID2020-113711GB-I00) and the Generalitat de Catalunya (Project 2017-SGR-39).

References

(1) Alexandrova, A. N.; Boldyrev, A. I.; Zhai, H.-J.; Wang, L.-S. All-Boron Aromatic Clusters as Potential New Inorganic Ligands and Building Blocks in Chemistry. *Coord. Chem. Rev.* **2006**, *250* (21), 2811–2866. https://doi.org/10.1016/j.ccr.2006.03.032.

(2) Zubarev, D. Y.; Boldyrev, A. I. Comprehensive Analysis of Chemical Bonding in Boron Clusters. *J. Comput. Chem.* **2007**, *28* (1), 251–268. https://doi.org/10.1002/jcc.20518.

(3) Zhang, Z.; Penev, E. S.; Yakobson, B. I. Two-Dimensional Boron: Structures, Properties and Applications. *Chem. Soc. Rev.* **2017**, *46* (22), 6746–6763. https://doi.org/10.1039/C7CS00261K.

(4) Barroso, J.; Pan, S.; Merino, G. Structural Transformations in Boron Clusters Induced by Metal Doping. *Chem. Soc. Rev.* **2022**, *51* (3), 1098–1123. https://doi.org/10.1039/D1CS00747E.

(5) Teixidor, F.; Viñas, C.; Demonceau, A.; Nuñez, R. Boron Clusters: Do They Receive the Deserved Interest? *Pure Appl. Chem.* **2003**, *75* (9), 1305–1313. https://doi.org/doi:10.1351/pac200375091305.

(6) Lipscomb, W. N. *Boron Hydrides*; W. A. Benjamin: New York, 1963.

(7) Lobayan, R. M.; Bochicchio, R. C.; Torre, A.; Lain, L. Electronic Structure and Effectively Unpaired Electron Density Topology in *closo*-Boranes: Nonclassical Three-Center Two-Electron Bonding. *J. Chem. Theory Comput.* **2011**, *7* (4), 979–987. https://doi.org/10.1021/ct100753q.

(8) Melichar, P.; Hnyk, D.; Fanfrlík, J. A Systematic Examination of Classical and Multi-Center Bonding in Heteroborane Clusters. *Phys. Chem. Chem. Phys.* **2018**, *20* (7), 4666–4675. https://doi.org/10.1039/C7CP07422K.

(9) Piazza, Z. A.; Hu, H.-S.; Li, W.-L.; Zhao, Y.-F.; Li, J.; Wang, L.-S. Planar Hexagonal B_{36} as a Potential Basis for Extended Single-Atom Layer Boron Sheets. *Nat. Commun.* **2014**, *5* (1), 3113. https://doi.org/10.1038/ncomms4113.

(10) Hou, C.; Tai, G.; Wu, Z.; Hao, J. Borophene: Current Status, Challenges and Opportunities. *Chempluschem* **2020**, *85* (9), 2186–2196. https://doi.org/10.1002/cplu.202000550.

(11) Duo, Y.; Xie, Z.; Wang, L.; Mahmood Abbasi, N.; Yang, T.; Li, Z.; Hu, G.; Zhang, H. Borophene-Based Biomedical Applications: Status and Future Challenges. *Coord. Chem. Rev.* **2021**, *427*, 213549. https://doi.org/10.1016/j.ccr.2020.213549.

(12) Murphy, N.; McCarthy, E.; Dwyer, R.; Farràs, P. Boron Clusters as Breast Cancer Therapeutics. *J. Inorg. Biochem.* **2021**, *218*, 111412. https://doi.org/10.1016/j.jinorgbio.2021.111412.

(13) Zhang, L.; Ye, Y.-L.; Li, X.-H.; Chen, J.-H.; Sun, W.-M. On the Potential of All-Boron Fullerene B_{40} as a Carrier for Anti-Cancer Drug Nitrosourea. *J. Mol. Liq.* **2021**, *342*, 117533. https://doi.org/10.1016/j.molliq.2021.117533.

(14) Hey-Hawkins, E.; Viñas Teixidor, C. *Boron-Based Compounds: Potential and Emerging Applications in Medicine*; Wiley: New York, 2018.

(15) Oleshkevich, E.; Morancho, A.; Saha, A.; Galenkamp, K. M. O.; Grayston, A.; Crich, S. G.; Alberti, D.; Protti, N.; Comella, J. X.; Teixidor, F.; Rosell, A.; Viñas, C. Combining Magnetic Nanoparticles and Icosahedral Boron Clusters in Biocompatible Inorganic Nanohybrids for Cancer Therapy. *Nanomed.: Nanotechnol. Biol. Med.* **2019**, *20*, 101986. https://doi.org/10.1016/j.nano.2019.03.008.

(16) Nuez-Martinez, M.; Pinto, C. I. G.; Guerreiro, J. F.; Mendes, F.; Marques, F.; Muñoz-Juan, A.; Xavier, J. A.; Laromaine, A.; Bitonto, V.; Protti, N.; Crich, S. G.; Teixidor, F.; Viñas, C. Cobaltabis(Dicarbollide) ($[o\text{-}COSAN]^-$) as Multifunctional Chemotherapeutics: A Prospective Application in Boron Neutron Capture Therapy (BNCT) for Glioblastoma. *Cancers* **2021**, *13* (24), 6367. https://doi.org/10.3390/cancers13246367.

(17) Barba-Bon, A.; Salluce, G.; Lostalé-Seijo, I.; Assaf, K. I.; Hennig, A.; Montenegro, J.; Nau, W. M. Boron Clusters as Broadband Membrane Carriers. *Nature* **2022**, *603* (7902), 637–642. https://doi.org/10.1038/s41586-022-04413-w.

(18) Scheifers, J. P.; Zhang, Y.; Fokwa, B. P. T. Boron: Enabling Exciting Metal-Rich Structures and Magnetic Properties. *Acc. Chem. Res.* **2017**, *50* (9), 2317–2325. https://doi.org/10.1021/acs.accounts.7b00268.

(19) Shao, W.; Tai, G.; Hou, C.; Wu, Z.; Wu, Z.; Liang, X. Borophene-Functionalized Magnetic Nanoparticles: Synthesis and Memory Device Application. *ACS Appl. Electron. Mater.* **2021**, *3* (3), 1133–1141. https://doi.org/10.1021/acsaelm.0c01004.

(20) Duret, G.; Quinlan, R.; Bisseret, P.; Blanchard, N. Boron Chemistry in a New Light. *Chem. Sci.* **2015**, *6* (10), 5366–5382. https://doi.org/10.1039/C5SC02207J.

(21) Nagamatsu, J.; Nakagawa, N.; Muranaka, T.; Zenitani, Y.; Akimitsu, J. Superconductivity at 39 K in Magnesium Diboride. *Nature* **2001**, *410* (6824), 63–64. https://doi.org/10.1038/35065039.

(22) Wang, Y.-J.; Xu, L.; Qiao, L.-H.; Ren, J.; Hou, X.-R.; Miao, C.-Q. Ultra-High Capacity Hydrogen Storage of B_6Be_2 and B_8Be_2 Clusters. *Int. J. Hydrogen Energy* **2020**, *45* (23),

12932–12939. https://doi.org/10.1016/j.ijhydene.2020.02.209.

(23) Du, J.; Jiang, G. An Aromatic Ca_2B_8 Complex for Reversible Hydrogen Storage. *Int. J. Hydrogen Energy* **2021**, *46* (36), 19023–19030. https://doi.org/10.1016/j.ijhydene.2021.03.060.

(24) Wang, Y.-J.; Wang, G.-L.; Guo, M.-M.; Miao, C.-Q.; Chen, H.-P.; Zhai, H.-J. The High-Capacity Hydrogen Storage of B_6Ca_2 and B_8Ca_2 Inverse Sandwiches. *Int. J. Hydrogen Energy* **2021**, *46* (47), 24225–24232. https://doi.org/10.1016/j.ijhydene.2021.04.206.

(25) Oña, O. B.; Torres-Vega, J. J.; Torre, A.; Lain, L.; Alcoba, D. R.; Vásquez-Espinal, A.; Tiznado, W. Chemical Bonding Analysis in Boron Clusters by Means of Localized Orbitals According to the Electron Localization Function Topology. *Theor. Chem. Acc.* **2015**, *134* (3), 28. https://doi.org/10.1007/s00214-015-1627-5.

(26) Arvanitidis, A. G.; Tai, T. B.; Nguyen, M. T.; Ceulemans, A. Quantum Rules for Planar Boron Nanoclusters. *Phys. Chem. Chem. Phys.* **2014**, *16* (34), 18311–18318. https://doi.org/10.1039/C4CP02323D.

(27) Yan, M.; Li, H.-R.; Zhao, X.-Y.; Lu, X.-Q.; Mu, Y.-W.; Lu, H.-G.; Li, S.-D. Fluxional Bonds in Planar B_{19}^-, Tubular Ta@B_{20}^-, and Cage-Like B_{39}^-. *J. Comput. Chem.* **2019**, *40* (9), 966–970. https://doi.org/10.1002/jcc.25728.

(28) Patouossa, I.; Arvanitidis, A. G.; Tshishimbi Muya, J.; Nguyen, M. T.; Ceulemans, A. Valence Bonds in Planar and Quasi-Planar Boron Disks. *Phys. Chem. Chem. Phys.* **2019**, *21* (2), 729–735. https://doi.org/10.1039/C8CP06749J.

(29) Li, R. S. ri.; You, X.-R.; Guo, J.-C.; Zhai, H.-J. Concentric Inner $2\pi/6\sigma$ and Outer $10\pi/14\sigma$ Aromaticity Underlies the Dynamic Structural Fluxionality of Planar B_{19}^- Wankel Motor Cluster. *J. Phys. Chem. A* **2021**, *125* (23), 5022–5030. https://doi.org/10.1021/acs.jpca.1c02764.

(30) Zubarev, D. Y.; Boldyrev, A. I. Chapter 5 - Multiple Aromaticity, Multiple Antiaromaticity, and Conflicting Aromaticity in Planar Clusters. In *Science Technology of Atomic*, Molecular, Condensed Matter & Biological Systems; Jena, P.; Castleman, A. W., Eds.; Elsevier, 2010; Vol. 1, pp 219–267. https://doi.org/10.1016/B978-0-444-53440-8.00005-7.

(31) Poater, J.; Solà, M.; Viñas, C.; Teixidor, F. π Aromaticity and Three-Dimensional Aromaticity: Two Sides of the Same Coin? *Angew. Chem. Int. Ed.* **2014**, *53* (45), 12191–12195. https://doi.org/10.1002/anie.201407359.

(32) Poater, J.; Solà, M.; Viñas, C.; Teixidor, F. Hückel's Rule of Aromaticity Categorizes Aromatic *closo* Boron Hydride Clusters. *Chem. – A Eur. J.* **2016**, *22* (22), 7437–7443. https://doi.org/10.1002/chem.201600510.

(33) Poater, J.; Viñas, C.; Bennour, I.; Escayola, S.; Solà, M.; Teixidor, F. Too Persistent to Give Up: Aromaticity in Boron Clusters Survives Radical Structural Changes. *J. Am. Chem. Soc.* **2020**, *142* (20), 9396–9407. https://doi.org/10.1021/jacs.0c02228.

(34) Poater, J.; Viñas, C.; Olid, D.; Solà, M.; Teixidor, F. Aromaticity and Extrusion of Benzenoids Linked to [o-COSAN]$^-$: Clar Has the Answer. *Angew. Chem. Int. Ed.* **2022**,

61 (134), e202200672. https://doi.org/10.1002/anie.202200672.

(35) Wang, Y.-J.; Guo, M.-M.; Wang, G.-L.; Miao, C.-Q.; Zhang, N.; Xue, T.-D. The Structure and Chemical Bonding in Inverse Sandwich B_6Ca_2 and B_8Ca_2 Clusters: Conflicting Aromaticity vs. Double Aromaticity. *Phys. Chem. Chem. Phys.* **2020**, *22* (36), 20362–20367. https://doi.org/10.1039/D0CP03703F.

(36) Feixas, F.; Matito, E.; Poater, J.; Solà, M. Rules of Aromaticity. In *Challenges and Advances in Computational Chemistry and Physics*; 2016; Vol. 22, pp 321–335. https://doi.org/10.1007/978-3-319-29022-5_12.

(37) Solà, M. Connecting and Combining Rules of Aromaticity. Towards a Unified Theory of Aromaticity. *WIREs Comput. Mol. Sci.* **2019**, *9* (4), e1404. https://doi.org/10.1002/wcms.1404.

(38) Hückel, E. Quantentheoretische Beiträge Zum Benzolproblem. *Z. Phys.* **1931**, *70* (3), 204–286. https://doi.org/10.1007/BF01339530.

(39) Baird, N. C. Quantum Organic Photochemistry. II. Resonance and Aromaticity in the Lowest $^3\pi\pi^*$ State of Cyclic Hydrocarbons. *J. Am. Chem. Soc.* **1972**, *94* (14), 4941–4948. https://doi.org/10.1021/ja00769a025.

(40) Ottosson, H. Exciting Excited-State Aromaticity. *Nat. Chem.* **2012**, *4* (12), 969–971. https://doi.org/10.1038/nchem.1518.

(41) Chen, D.; Szczepanik, D. W.; Zhu, J.; Solà, M. All-Metal Baird Aromaticity. *Chem. Commun.* **2020**, *56* (83), 12522–12525. https://doi.org/10.1039/D0CC05586G.

(42) Duong, L. Van; Pham, H. T.; Tam, N. M.; Nguyen, M. T. A Particle on a Hollow Cylinder: The Triple Ring Tubular Cluster B_{27}^+. *Phys. Chem. Chem. Phys.* **2014**, *16* (36), 19470–19478. https://doi.org/10.1039/C4CP01996B.

(43) Pham, H. T.; Lim, K. Z.; Havenith, R. W. A.; Nguyen, M. T. Aromatic Character of Planar Boron-Based Clusters Revisited by Ring Current Calculations. *Phys. Chem. Chem. Phys.* **2016**, *18* (17), 11919–11931. https://doi.org/10.1039/c5cp07391j.

(44) Mandado, M.; Graña, A. M.; Pérez-Juste, I. Aromaticity in Spin-Polarized Systems: Can Rings Be Simultaneously Alpha Aromatic and Beta Antiaromatic? *J. Chem. Phys.* **2008**, *129* (16), 164114. https://doi.org/10.1063/1.2999562.

(45) Soncini, A.; Fowler, P. W. Counter-Rotating Spin-Polarised Ring Currents in Odd-Electron Carbocycles. *Chem. – A Eur. J.* **2013**, *19* (5), 1740–1746. https://doi.org/10.1002/chem.201202572.

(46) Valiev, R. R.; Kurten, T.; Valiulina, L. I.; Ketkov, S. Y.; Cherepanov, V. N.; Dimitrova, M.; Sundholm, D. Magnetically Induced Ring Currents in Metallocenothiaporphyrins. *Phys. Chem. Chem. Phys.* **2022**, *24* (3), 1666–1674. https://doi.org/10.1039/D1CP04779E.

(47) Tai, T. B.; Ceulemans, A.; Nguyen, M. T. Disk Aromaticity of the Planar and Fluxional Anionic Boron Clusters $B_{20}^{-/2-}$. *Chem. – A Eur. J.* **2012**, *18* (15), 4510–4512. https://doi.org/10.1002/chem.201104064.

(48) Tai, T. B.; Havenith, R. W. A.; Teunissen, J. L.; Dok, A. R.; Hallaert, S. D.; Nguyen, M. T.; Ceulemans, A. Particle on a Boron Disk: Ring Currents and Disk Aromaticity in B_{20}^{2-}. *Inorg. Chem.* **2013**, *52* (18), 10595–10600. https://doi.org/10.1021/ic401596s.

(49) Islas, R.; Inostroza, D.; Arias-Olivares, D.; Zúñiga-Gutiérrez, B.; Poater, J.; Solà, M. Analysis of the Electronic Delocalization in Some Isoelectronic Analogues of B_{12} Doped with Beryllium and/or Carbon. *Phys. Chem. Chem. Phys.* **2020**, *22* (21), 12245–12259. https://doi.org/10.1039/D0CP01844A.

(50) Fowler, J. E.; Ugalde, J. M. The Curiously Stable Cluster B_{13}^{+} and Its Neutral and Anionic Counterparts: The Advantages of Planarity. *J. Phys. Chem. A* **2000**, *104* (2), 397–403. https://doi.org/10.1021/jp991957v.

(51) Jiménez-Halla, J. O. C.; Islas, R.; Heine, T.; Merino, G. B_{19}^{-}: An Aromatic Wankel Motor. *Angew. Chem. Int. Ed.* **2010**, *49* (33), 5668–5671. https://doi.org/10.1002/anie.201001275.

(52) Jalife, S.; Liu, L.; Pan, S.; Cabellos, J. L.; Osorio, E.; Lu, C.; Heine, T.; Donald, K. J.; Merino, G. Dynamical Behavior of Boron Clusters. *Nanoscale* **2016**, *8* (40), 17639–17644. https://doi.org/10.1039/C6NR06383G.

(53) Zubarev, D. Y.; Boldyrev, A. I. Developing Paradigms of Chemical Bonding: Adaptive Natural Density Partitioning. *Phys. Chem. Chem. Phys.* **2008**, *10* (34), 5207–5217. https://doi.org/10.1039/B804083D.

(54) Lazzeretti, P. Assessment of Aromaticity via Molecular Response Properties. *Phys. Chem. Chem. Phys.* **2004**, *6* (2), 217–223. https://doi.org/10.1039/B311178D.

(55) Sundholm, D.; Fliegl, H.; Berger, R. J. F. Calculations of Magnetically Induced Current Densities: Theory and Applications. *WIREs Comput. Mol. Sci.* **2016**, *6* (6), 639–678. https://doi.org/10.1002/wcms.1270.

(56) Sundholm, D.; Dimitrova, M.; Berger, R. J. F. Current Density and Molecular Magnetic Properties. *Chem. Commun.* **2021**, *57* (93), 12362–12378. https://doi.org/10.1039/D1CC03350F.

(57) Frisch, M. J.; Trucks, G. W.; Schlegel, H. B.; Scuseria, G. E.; Robb, M. A.; Cheeseman, J. R.; Scalmani, G.; Barone, V.; Mennucci, B.; Petersson, G. A.; Nakatsuji, H.; Caricato, M.; Li, X.; Hratchian, H. P.; Izmaylov, A. F.; Bloino, J.; Zheng, G.; Sonnenberg, J. L.; Hada, M.; Ehara, M.; Toyota, K.; Fukuda, R.; Hasegawa, J.; Ishida, M.; Nakajima, T.; Honda, Y.; Kitao, O.; Nakai, H.; Vreven, T.; Montgomery, J. A.; Peralta, J. E.; Ogliaro, F.; Bearpark, M.; Heyd, J. J.; Brothers, E.; Kudin, K. N.; Staroverov, V. N.; Kobayashi, R.; Normand, J.; Raghavachari, K.; Rendell, A.; Burant, J. C.; Iyengar, S. S.; Tomasi, J.; Cossi, M.; Rega, N.; Millam, J. M.; Klene, M.; Knox, J. E.; Cross, J. B.; Bakken, V.; Adamo, C.; Jaramillo, J.; Gomperts, R.; Stratmann, R. E.; Yazyev, O.; Austin, A. J.; Cammi, R.; Pomelli, C.; Ochterski, J. W.; Martin, R. L.; Morokuma, K.; Zakrzewski, V. G.; Voth, G. A.; Salvador, P.; Dannenberg, J. J.; Dapprich, S.; Daniels, A. D.; Farkas; Foresman, J. B.; Ortiz, J. V; Cioslowski, J.; Fox, D. J. Gaussian 09, Revision B.01. *Gaussian Inc.*, Wallingford CT 2009.

(58) Keith, T. A.; Bader, R. F. W. Calculation of Magnetic Response Properties Using a

Continuous Set of Gauge Transformations. *Chem. Phys. Lett.* **1993**, *210* (1–3), 223–231. https://doi.org/10.1016/0009-2614(93)89127-4.

(59) Keith, T. A.; Bader, R. F. W. Topological Analysis of Magnetically Induced Molecular Current Distributions. *J. Chem. Phys.* **1993**, *99* (5), 3669–3682. https://doi.org/10.1016/0009-2614(94)00158-8.

(60) Lazzeretti, P.; Malagoli, M.; Zanasi, R. Computational Approach to Molecular Magnetic Properties by Continuous Transformation of the Origin of the Current Density. *Chem. Phys. Lett.* **1994**, *220* (3–5), 299–304. https://doi.org/10.1016/0009-2614(94)00158-8.

(61) Lazzeretti, P. Methods of Continuous Translation of the Origin of the Current Density Revisited. *Theor. Chem. Acc.* **2012**, *131* (5), 1222. https://doi.org/10.1007/s00214-012-1222-y.

(62) Ayachit, U. *The ParaView Guide: A Parallel Visualization Application*; Kitware, 2015.

(63) Irons, T. J. P.; Spence, L.; David, G.; Speake, B. T.; Helgaker, T.; Teale, A. M. Analyzing Magnetically Induced Currents in Molecular Systems Using Current-Density-Functional Theory. *J. Phys. Chem. A* **2020**, *124* (7), 1321–1333. https://doi.org/10.1021/acs.jpca.9b10833.

(64) Elhay, S.; Kautsky, J. Algorithm 655: IQPACK: FORTRAN Subroutines for the Weights of Interpolatory Quadratures. *ACM Trans. Math. Softw.* **1987**, *13* (4), 399–415. https://doi.org/10.1145/35078.214351.

(65) Pyykkö, P. Additive Covalent Radii for Single-, Double-, and Triple-Bonded Molecules and Tetrahedrally Bonded Crystals: A Summary. *J. Phys. Chem. A* **2015**, *119* (11), 2326–2337. https://doi.org/10.1021/jp5065819.

(66) An, W.; Bulusu, S.; Gao, Y.; Zeng, X. C. Relative Stability of Planar versus Double-Ring Tubular Isomers of Neutral and Anionic Boron Cluster B_{20} and B_{20}^-. *J. Chem. Phys.* **2006**, *124* (15), 154310. https://doi.org/10.1063/1.2187003.

(67) Oger, E.; Crawford, N. R. M.; Kelting, R.; Weis, P.; Kappes, M. M.; Ahlrichs, R. Boron Cluster Cations: Transition from Planar to Cylindrical Structures. *Angew. Chem. Int. Ed.* **2007**, *46* (44), 8503–8506. https://doi.org/10.1002/anie.200701915.

(68) Kiran, B.; Bulusu, S.; Zhai, H. J.; Yoo, S.; Zeng, X. C.; Wang, L. S. Planar-to-Tubular Structural Transition in Boron Clusters: B_{20} as the Embryo of Single-Walled Boron Nanotubes. *Proc. Natl. Acad. Sci. U. S. A.* **2005**, *102* (4), 961–964. https://doi.org/10.1073/pnas.0408132102.

(69) Fowler, P. W.; Gray, B. R. Induced Currents and Electron Counting in Aromatic Boron Wheels: B_8^{2-} and B_9^-. *Inorg. Chem.* **2007**, *46* (7), 2892–2897. https://doi.org/10.1021/ic062302t.

Table of Contents Graphic